

# Salt-concentration dependence of the structure and form factors for the wormlike micelle made from a dual surfactant in aqueous solutions

Kenichi Eguchi,<sup>a</sup> Isamu Kaneda,<sup>b</sup> Yoshiko Hiwatari,<sup>b</sup> Hiroyasu Masunaga<sup>c</sup> and Kazuo Sakurai<sup>a\*</sup>

<sup>a</sup>The University of Kitakyushu, Fukuoka 808-0132, Japan, <sup>b</sup>Shiseido Research Center, Polymer Science Research Laboratories, Kanagawa 224-8558, Japan, and <sup>c</sup>Japan Synchrotron Radiation Research Institute (JASRI/SPring-8), Hyogo 679-5198, Japan. Correspondence e-mail: sakurai@env.kitakyu-u.ac.jp

Small-angle X-ray scattering (SAXS) from dual-surfactant aqueous solutions made from sodium lauryl ether sulfate and coconut fatty acid amido propyl betaine was systematically measured as a function of the net sodium cation concentration,  $[\text{Na}^+]^*$ , and the surfactant concentration,  $C_D$ . The SAXS intensity  $[I(q)]$  was normalized to  $C_D$  and the resultant  $I(q)/C_D$  was extrapolated to  $C_D = 0$  to give a form factor  $P(q)$  for each  $[\text{Na}^+]^*$  [where  $q = 4\pi\sin(\theta/2)/\lambda$  is the magnitude of the scattering vector,  $\lambda$  is the wavelength and  $2\theta$  is the scattering angle]. The low- $q$  behaviour of  $P(q)$  was consistent with long rigid cylinders. The middle- and high- $q$  profiles fitted well with a core-shell cylinder model for all  $[\text{Na}^+]^*$ . The core and total radii ( $R_c$  and  $R_s$ ) did not depend on  $[\text{Na}^+]^*$  at all:  $R_c = 1.2 \pm 0.05$  and  $R_s = 3.1 \pm 0.05$  nm for  $[\text{Na}^+]^* = 0.42\text{--}1.5$  mol l<sup>-1</sup>, indicating that the salt concentration changes did not induce any structural changes and re-assembling of the surfactants comprising the micelles. This fact is in contrast to the rheological behaviour where the relaxation mode strongly depends on  $[\text{Na}^+]^*$ . The structure factor  $[S(q)]$  was obtained by dividing  $I(q)/C_D$  by  $P(q)$  for each  $C_D$  and the mean distance ( $d_m$ ) between the micelles was obtained from the first maximum of  $S(q)$  versus  $q$  plots. The  $d_m$  value decreased with increasing  $C_D$  and  $[\text{Na}^+]^*$ , which is in good agreement with the theoretical prediction and experimental results for charged wormlike micelle solutions.

© 2007 International Union of Crystallography  
Printed in Singapore – all rights reserved

## 1. Introduction

Sodium lauryl ether sulfate (LES) and coconut fatty acid amido propyl betaine (AMPB) are the most common ingredients of shampoo [the chemical structures of which are presented in the inset of Fig. 3 of Hiwatari *et al.* (2004)]. The surfactants are mixed together to tune detergency and other properties for final products. Understanding the rheological properties of the mixed-surfactant aqueous solutions is essential for practical applications and, thus, there have been many studies on this issue (Mu *et al.*, 2002). However, as far as we know, there are only a few studies which focus on the relationship between rheology and micellar structure (Acharya *et al.*, 2006). This paper presents synchrotron small-angle X-ray scattering (SAXS) results for LES/AMPB dual-component aqueous solutions and explores the micellar structures and inter-micellar interactions as a function of the salt and surfactant concentrations.

Being similar to other surfactant aqueous solutions, the LES/AMPB/water system shows viscoelastic behaviour characteristic of micelle solutions. The viscoelasticity strongly depends on the micelle structures and inter-micellar interactions such as entanglement and electrostatic repulsion. Since LES is an anionic surfactant, the micellar structures are mainly determined by the counter cation concentration. Increase of the salt concentration enhances electrostatic shielding effects, which reduce repulsion between the ionic headgroups and thus induce the structural transition of micelles.

Generally, the transition is from spherical to cylindrical micelles, and by increasing the cylinder length, the cylindrical micelles start to behave as wormlike chains. When the contour length of the cylinder becomes long enough to form entanglement between the cylinders, the characteristic viscoelasticity emerges (Shikata *et al.*, 1987).

Fig. 1 plots the zero-shear viscosity ( $\eta$ ) against the net sodium cation concentration,  $[\text{Na}^+]^*$ , where the total surfactant concentration (hereinafter denoted by  $C_D$  and LES:AMPB is fixed at 5:3 by weight ratio) is 8 wt% (203 mmol l<sup>-1</sup>) (Eguchi & Sakurai, 2007). The viscosity dramatically increases in the  $[\text{Na}^+]^*$  range 0–0.75 mol l<sup>-1</sup> and showed a broad maximum at around 1.1 mol l<sup>-1</sup>. Dynamic viscoelastic measurements were carried out at  $[\text{Na}^+]^* > 0.75$  mol l<sup>-1</sup>. Except for high  $C_D$  samples, the simple Maxwell model with a single relaxation time ( $\tau$ ) could describe the frequency dependence of the modulus and the plateau modulus as proportional to  $C_D^2$  (data not shown). These two facts indicate that the origin of the elasticity was the entanglements of the infinitely long wormlike micelles (Ferry, 1980). We found that there are three regions that show different  $C_D$  dependence on  $\tau$ . As presented in the inset of Fig. 1, at  $[\text{Na}^+]^* = 1.0$  (except for  $C_D > 0.5$  mol l<sup>-1</sup>), 1.25 and 1.50 mol l<sup>-1</sup>,  $\tau$  became independent of  $C_D$ , indicating that two micelles can cross with each other, the so-called phantom crossing proposed by Shikata *et al.* (1988). The value of  $\tau$  decreased with increasing  $[\text{Na}^+]^*$ , suggesting that the lifetime of the junction of micelles (tentatively formed when the micelles cross with each other) decreased with increasing  $[\text{Na}^+]^*$ . We

presumed that the decreasing lifetime of the junction should be related to structural changes of the micelles. At  $[\text{Na}^+]^* = 0.75 \text{ mol l}^{-1}$  and  $C_D < 0.5 \text{ mol l}^{-1}$ ,  $\tau \propto C_D^{0.5}$  was seemingly held. This concentration dependence cannot be rationalized by a simple model. At higher  $C_D$  ( $> 0.61 \text{ mol l}^{-1}$ ), for  $[\text{Na}^+]^* = 0.75$  and  $1.0 \text{ mol l}^{-1}$ , a dramatic increase in  $\tau$  was observed. As a matter of fact, in this region, both storage and loss moduli could not be fitted with the simple Maxwell model and thus we plotted the longest relaxation time in Fig. 1. The increased relaxation time and deviation from the single relaxation time should be related to the appearance of another relaxation mode, rather than micellar entanglement relaxation. When we prepared samples with larger  $C_D$  and/or  $[\text{Na}^+]^*$  than this region (for example at  $C_D = 0.7 \text{ mol l}^{-1}$  and  $[\text{Na}^+]^* = 1.0 \text{ mol l}^{-1}$ ), liquid–liquid phase separation was observed. Therefore, the origin of the slow relaxation is presumably ascribed to composition fluctuation that becomes large near a phase boundary.

As described above, the viscoelastic nature of the present system strongly depends on  $[\text{Na}^+]^*$  and apparently should be related to structural changes of the micelles. The aim of this paper is to examine the micellar structures and inter-micellar interactions by comparing with rheological properties.

## 2. Experiments

LES and AMPB were purchased from Toho Chemical Industry Co. Ltd and Sanyo Kasei Industry Co. Ltd, respectively, and used without further purification. The composition ratio of LES:AMPB was always fixed at a 5:3 weight ratio. The counter cation of LES is  $\text{Na}^+$  and  $[\text{Na}^+]^*$  is defined as the total amount of  $\text{Na}^+$  (added NaCl and the counter  $\text{Na}^+$ ). SAXS measurements were carried out at 40B2 SPring-8 using a 1.5 m camera and a Rigaku imaging plate ( $30 \times 30 \text{ cm}$ ,  $1000 \times 1000$  pixels). The exposure time was 20 min and the relative X-ray intensity and the sample transmittance were determined with ion chambers located in front of or behind the sample. A quartz capillary cell (2 mm diameter, Hilgenberg GmbH) was used for the scattering cell. For all measurements including the solvents we used the same cell. We subtracted the solvent scattering from the sample scattering by use of the following equation:

$$I(q) = I_{\text{sample}}(q) \frac{1}{TX_{\text{in}}} - V_f \left[ [\text{Na}^+]^* \frac{I_{\text{NaOH}}(q)}{TX_{\text{in}}} + [\text{Cl}^-]^* \frac{I_{\text{Cl}}(q)}{TX_{\text{in}}} + \frac{I_{\text{water}}(q)}{TX_{\text{in}}} \right]. \quad (1)$$

$q$  is given by  $4\pi\sin(\theta/2)/\lambda$ , where  $\theta$  is the scattering angle and  $\lambda$  is the X-ray wavelength.  $I_{\text{NaOH}}$  and  $I_{\text{HCl}}$  denote the molar scattering from NaOH and HCl solutions, respectively,  $I_{\text{water}}$  is that from water itself,  $V_f$  is the volume fraction of the solvent,  $T$  is the transmittance and  $X_{\text{in}}$  is the read value of the ion chamber in front of the sample when the measurement was carried out.

## 3. Theoretical background and SAXS data analysis

$I(q)$  from isotropic solutions containing cylindrical micelles can be written as

$$I(q) = kP(q)S(q). \quad (2)$$

Here,  $k$  is the averaged number of micelles and proportional to  $C_D$  when  $C_D$  is much larger than the critical micelle concentration (CMC); in our case the CMC was  $4.8 \times 10^{-3} \text{ mol l}^{-1}$ .  $P(q)$  and  $S(q)$  are the form and structural factors, respectively. For the spherical particles,  $S(q)$  can be analytically calculated if an appropriate inter-particle interaction potential is given. On the other hand, for randomly oriented rodlike or wormlike micelles, the calculation becomes difficult. Recently, Cannavacciuolo *et al.* (2002) presented an extensive Monte Carlo study on charged wormlike micelles to calculate  $S(q)$ . To obtain  $P(q)$  from the observed data,  $I(q)/C_D$  was extrapolated to the limit  $C_D \rightarrow 0$ . This is because  $S(q) = 1$  for all  $q$  at  $C_D = 0$ . Once  $P(q)$  is obtained,  $S(q)$  can be evaluated by dividing  $I(q)/C_D$  with  $P(q)$ .

As a matter of fact, this extrapolation does not always work, because the length of the wormlike micelles depends on  $C_D$ ; the length decreases with decreasing  $C_D$ . However, in our  $q$  range, we did not observe any influence from the overall size change. This is because that the overall size has an influence on the form factor in the  $q$  range less than approximately  $q \sim 1/L$ , where  $L$  is the contour length of the micelle. Viscosity data indicated that the micelle length is long in the all concentrations measured using SAXS. Therefore, the above-mentioned extrapolation should work reasonably. In fact,  $I(q)/C_D$  versus  $q$  profiles could be almost superimposed with each other when  $C_D < 0.03 \text{ mol l}^{-1}$ , showing that the above discussion is correct. Fig. 2 presents an example of the extrapolation where  $[\text{Na}^+]^* = 0.42 \text{ mol l}^{-1}$ . In the range of  $q > 0.33 \text{ nm}^{-1}$ ,  $I(q)/C_D$  is essentially identical. We obtained the values of  $I(q)/C_D$  at  $C_D = 0 \text{ mol l}^{-1}$  for all  $q < 0.33 \text{ nm}^{-1}$  (Fig. 2 does not show all of them to avoid confusion).

In this paper, we found that the obtained  $P(q)$  can be described well with a core–shell cylinder model of infinite length:

$$P(q) = \int_{-\infty}^{\infty} P(q, r) \exp\left(-\frac{r^2}{2\sigma^2}\right) dr / \sqrt{2\pi}\sigma, \quad (3)$$

$$P(q, r) = \frac{1}{q} \left\{ V_s \frac{J_1(qR_s + qr)}{q(R_s + r)} + V_c \frac{J_1[qR_c + (R_c/R_s)qr]}{q[R_c + (R_c/R_s)r]} \right\}^2, \quad (4)$$

where  $\sigma$  is the standard deviation,  $J_1(x)$  is the first-order Bessel function,  $R_c$  and  $R_s$  are the core and total (core + shell) radii, and  $V_c$  and  $V_s$  are the parameters related to the electron density differences between the core and the shell, and the shell and the solvent

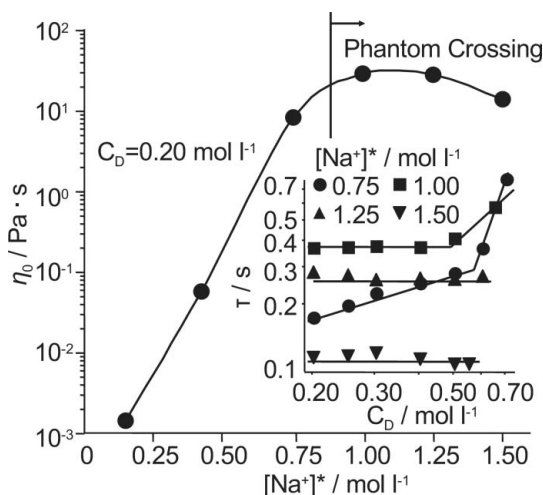
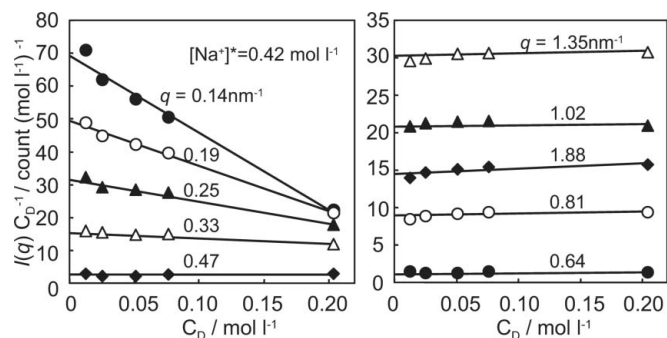


Figure 1

$[\text{Na}^+]^*$  dependence of the zero-shear viscosity for the LES/AMPB/water system at  $C_D = 0.20 \text{ mol l}^{-1}$ , measured with a B-type viscometer (DV-1+, Brookfield). The inset shows the  $C_D$  dependence of  $\tau$  determined with dynamic viscosity measurements for the four  $[\text{Na}^+]^*$  concentrations more than  $0.75 \text{ mol l}^{-1}$ .



**Figure 2** Examples for the extrapolation to zero concentration for  $[\text{Na}^+]^* = 0.42 \text{ mol l}^{-1}$ . In the case of  $q > 0.33 \text{ nm}^{-1}$ ,  $I(q)/C_D$  became almost independent of  $C_D$ .

(Pedersen, 1997). In equation (4), we assumed that the distributions of  $R_c$  and  $R_s$  are not independent for convenience.

### 4. Results and discussion

#### 4.1. Form factors

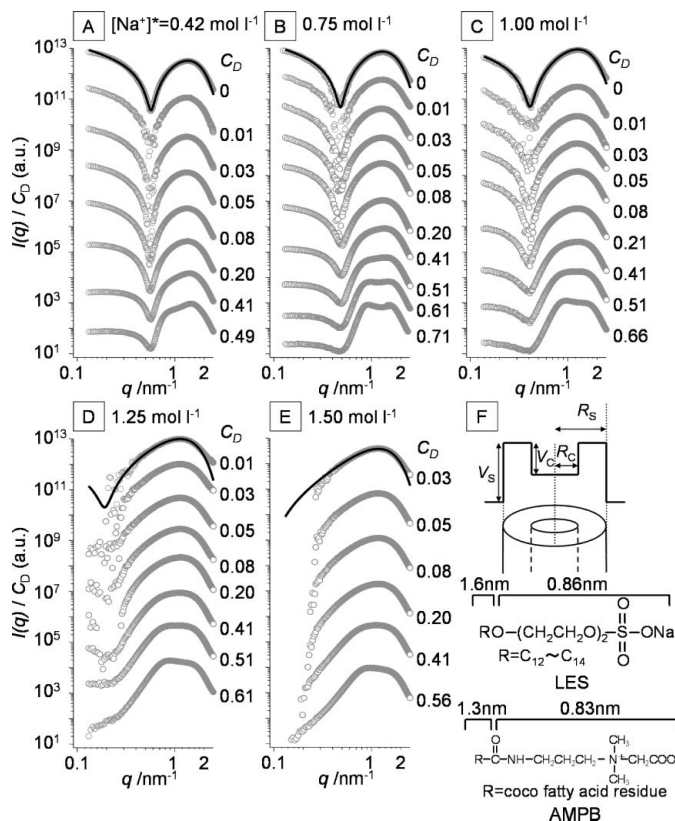
Panels A–E in Fig. 3 present  $I(q)/C_D$  at different  $C_D$  for each  $[\text{Na}^+]^*$ . For all  $[\text{Na}^+]^*$ , with increasing  $C_D$  the low- $q$  intensities decreased and a shoulder appeared around  $q = 0.8\text{--}1.0 \text{ nm}^{-1}$ . This feature can be ascribed to concentration effects, indicating that intermicellar diffraction becomes appreciable. It is interesting that the scattering profiles were drastically changed with increasing  $[\text{Na}^+]^*$ , especially for the low- $q$  profiles. This feature may be ascribed to both micelle structural changes and the electron density changes of the solvent. For  $[\text{Na}^+]^* = 0.42, 0.75$  and  $1.00 \text{ mol l}^{-1}$ , extrapolation to  $C_D = 0$  could be carried out numerically and the resultant profiles [hereinafter denoted by  $I(q)_{C=0}$ ] are shown at the top of each panel. For  $[\text{Na}^+]^* = 1.25$  and  $1.50 \text{ mol l}^{-1}$ , we could not extrapolate the data because the intensities in the low- $q$  region were too weak.

Fig. 4 presents the cross-sectional plots of  $I(q)_{C=0}$  for  $[\text{Na}^+]^* = 0.42, 0.75$  and  $1.0 \text{ mol l}^{-1}$ . At  $q^2 < 0.05 \text{ nm}^{-2}$ , the data points can be fitted by a straight line. This feature indicates that  $I(q)_{C=0}$  shows the asymptotic behaviour of  $I(q) \sim 1/q$  in the low- $q$  region which is expected for rodlike scattering objects. From the slope of the data, we calculated the cross-sectional radius of gyration ( $R_{gc}$ ) by use of the following equation:

$$I(q) \propto \frac{1}{q} \exp\left(\frac{-q^2 R_{gc}^2}{2}\right). \quad (5)$$

The resultant values are presented at the right side of Fig. 4, showing that  $R_{gc}$  increased from 2.75 to 5.34 nm with increasing  $[\text{Na}^+]^*$ . For a uniform cylindrical particle with a radius of  $R$ ,  $R_{gc}$  is given by  $R/2^{1/2}$ , which leads to the result that  $R$  increased from 3.9 to 7.5 nm. Interpretation of this result will be discussed later. According to previous studies that measured neutron scattering from wormlike micelles (Schurtenberger *et al.*, 1991; Jerke *et al.*, 1998), the exponent  $\alpha$  in  $P(q) \propto q^{-\alpha}$  changes from 1 to 2 with decreasing  $q$ . This transition occurs at  $q \times l_p \simeq 1.9$  (where  $l_p$  is the persistence length of the wormlike micelles) (Schurtenberger *et al.*, 1991). We did not observe such a transition. This is because our minimum  $q$  is too large to observe this change of  $\alpha$ . Therefore, we can conclude that  $P(q)$  is controlled by distances over which the micelles are rodlike rather than flexible.

To describe  $I(q)_{C=0}$ , we adopted a core-shell cylinder model with infinite length [equation (4)]. Since our  $q$  range is much larger than  $1/L$  and  $1/l_p$ , we considered that infinite cylinders are suitable. In



**Figure 3** Panels A–E:  $C_D$  dependence of  $I(q)/C_D$  and the  $P(q)$  profiles that were obtained by the extrapolation of  $C_D = 0$ , and comparison with the theoretical calculation (solid lines) based on the core-shell cylinder model with  $R_c = 1.2 \text{ nm}$ ,  $R_s = 3.1 \text{ nm}$  and  $V_c = -10$ . Panel F: the schematic illustration of the core-shell cylinder model and illustration of the definitions of the structural parameters; the perpendicular direction is the electron density. The chemical structures of LES and AMPB, and their sizes are also presented.

equation (4), the electron density in the cylindrical micelles varies in a rectangular manner at the interface between the core and the shell, and between the shell and the solvent. The core and shell regions presumably consist mainly of the surfactant tails and head groups, respectively. To obtain the best-fit parameters, we have used two consecutive procedures. In the first step, we have used a homogeneous cylinder model (*i.e.*  $\sigma = 0$ ) and obtained a set of the best-fit parameters of  $R_c$ ,  $R_s$ ,  $V_c$  and  $V_s$  by an iteration method. In the second step, the appropriate  $\sigma$  values were determined and then fine tuning

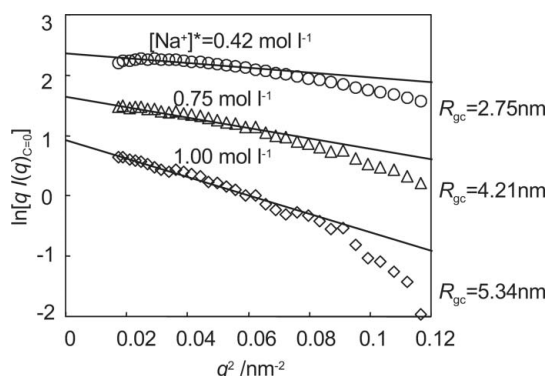


**Figure 4** Plots of  $\ln[qI(q)_{C=0}]$  versus  $q^2$  (cross-sectional plot) at different  $[\text{Na}^+]^*$  and the linear fit to the low- $q$  region which was used to determine  $R_{gc}$ .

**Table 1**

The obtained core-shell cylinder parameters used to fit the form factors.

$[\text{Na}^+]^*$	$R_s$ (nm)	$R_c$ (nm)	$V_s$	$V_c$	$\sigma$ (nm)
0.42	3.0	1.2	14.1	-10	0.23
0.75	3.1	1.2	12.9	-10	0.23
1.00	3.1	1.2	12.0	-10	0.28
1.25	3.1	1.2	11.1	-10	0.25
1.50	3.1	1.2	10.2	-10	0.25

of  $R_c$ ,  $R_s$ ,  $V_c$  and  $V_s$  was carried out. The parameters obtained are presented in Table 1 and shown plotted against  $[\text{Na}^+]^*$  in Fig. 5. Here, the error of the estimation was within  $\pm 0.05$  nm for both  $R_c$  and  $R_s$ . The solid lines in panels A–C (Fig. 3) show the calculated values of  $P(q)$  from equations (3) and (4) using the parameters in Table 1, compared with the experimental data of  $I(q)_{C=0}$ . The calculated values agree with the experimental data very well.

It is interesting that  $R_c$  and  $R_s$  do not depend on  $[\text{Na}^+]^*$ , when  $R_c = 1.2$  nm and  $R_s = 3.1$  nm for  $[\text{Na}^+]^* = 0.42, 0.75$  and  $1.00$  mol l<sup>-1</sup>. The only structural parameter affected by  $[\text{Na}^+]^*$  was  $V_s$ , and the relation of  $V_s$  and  $[\text{Na}^+]^*$  can be fitted by a straight line. Since  $R_c$ ,  $R_s$  and  $V_c$  are independent of  $[\text{Na}^+]^*$  and the linear relation between  $V_s$  and  $[\text{Na}^+]^*$  is held, we can predict the parameter sets for  $[\text{Na}^+]^* = 1.25$  and  $1.5$  mol l<sup>-1</sup>, and the results are presented in Table 1. Based on these parameters, we calculated the theoretical  $P(q)$  for each and compared them with that of  $C_D = 13$  or  $25$  mmol l<sup>-1</sup> for  $[\text{Na}^+]^* = 1.25$  and  $1.5$  mol l<sup>-1</sup> in panels D and E, respectively. Here the concentration effect can be considered negligibly small for these  $C_D$ . For both cases, agreement between the theoretical prediction and experiment is good enough to conclude that the predicted parameters are reliable.

The values of  $R_s$  and  $R_c$  are found to be comparable with those of the headgroups and tails for LES and AMPB molecules (see Fig. 3 for the size of the molecules), confirming that they form conventional cylindrical micelles. The unchanged  $R_s$ ,  $R_c$  and  $V_c$  mean that the local molecular packing between the headgroups is not changed by  $[\text{Na}^+]^*$ . In fact, this conclusion is rather surprising because we expected that the reduced electrostatic repulsion might bring the headgroups close to each other, or at least the structural parameters might be changed corresponding to decreasing lifetime of the entanglement junction (see the inset of Fig. 1). With increasing  $[\text{Na}^+]^*$ , the scattering intensities in the low- $q$  range dramatically drop as presented in Fig. 2, panels D and E. These changes are not owing to the structural changes of the cross section of the micelle, but should be ascribed to the electron density increment of the solvent, which decreases  $V_s$ , as schematically presented in the inset of Fig. 3.

Fig. 4 showed that  $R_{gc}$  decreased with increasing  $[\text{Na}^+]^*$ . This change did not reflect the dimensional changes of the micelles, but the

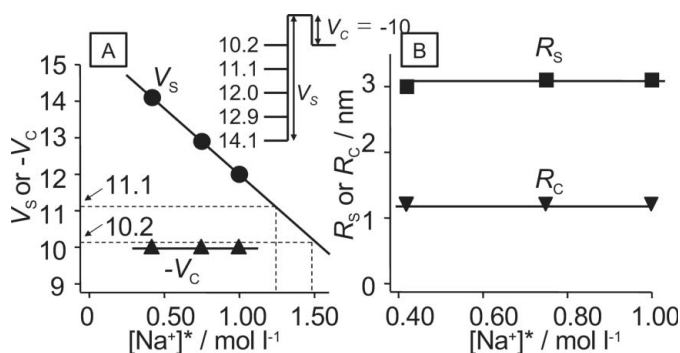


**Figure 5**  
 $[\text{Na}^+]^*$  dependence of the structural parameters and schematic comparison of  $V_s$  and  $V_c$ .

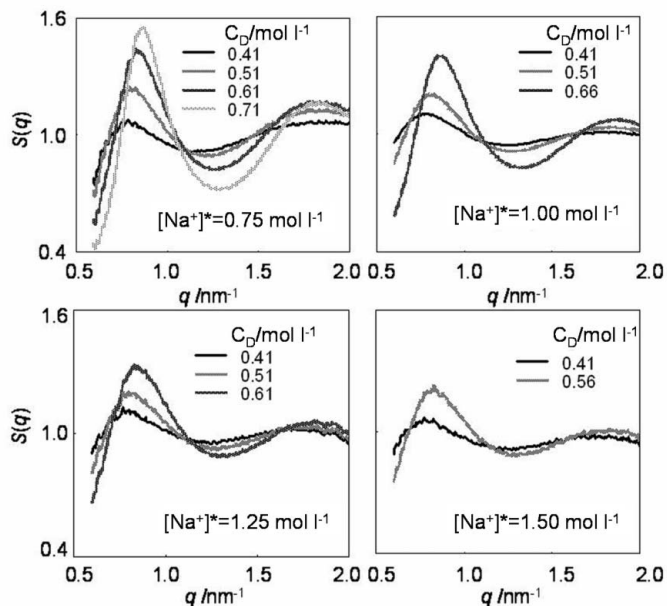


**Figure 6**  
 $C_D$  dependence of the  $S^*(q)$  profiles for  $[\text{Na}^+]^* = 0.75, 1.00, 1.25$  and  $1.50$  mol l<sup>-1</sup>. The number attached to each profile is  $C_D$  in mol l<sup>-1</sup>.

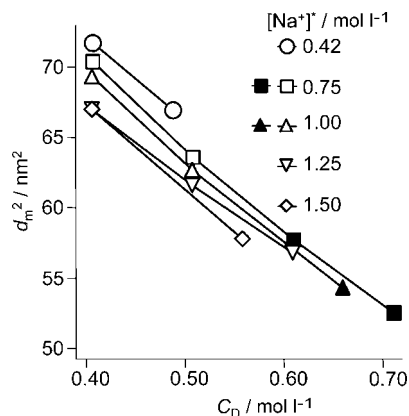


**Figure 7**  
 $C_D$  dependence of  $d_m$  for all  $[\text{Na}^+]^*$  samples. The filled marks indicate the presence of slow relaxations observed with rheological measurements.

change of salt concentration of the solvent. With increasing  $[\text{Na}^+]^*$ , the electron density of the solvent becomes close to that of the core, as presented in the inset of Fig. 5. The origin of the contrast for SAXS from solutions is the electron density difference between the scattering objects and solvents. Therefore, the situation in which the core and solvent have a close electron density provides strong contrast to the shell. This is the reason that  $R_{gc}$  increased with increasing  $[\text{Na}^+]^*$ .

**4.2. Structure factors**

Fig. 6 presents  $S(q)$  obtained from equation (2) for  $[\text{Na}^+]^* = 0.75, 1.00, 1.25$  and  $1.50$  mol l<sup>-1</sup>. For each case, with increasing  $C_D$  the intensity of the first maximum increases and the peak position shifts to higher  $q$ , and the second one becomes appreciable. This feature can be considered as a sign of formation of a local order in the system and is a well known feature also observed in polyelectrolyte solutions. Using the Bragg equation, the mean distance between the micelles ( $d_m$ ) was determined for each  $C_D$  and plotted against  $C_D$  for all

$[\text{Na}^+]^*$  in Fig. 7. The  $d_m$  value decreased with increasing  $C_D$ . This means that the micelles are, on average, closer to each other with increasing  $C_D$ . A similar shift of  $d_m$  is observed at fixed  $C_D$  and with increasing  $[\text{Na}^+]^*$ . In this case, the decrease of  $d_m$  may be considered due to the weakening of the electrostatic repulsion as the screening is increased. Furthermore, the peak height (which is related to the order of a structure) seems to decrease with increasing  $[\text{Na}^+]^*$ . These two results suggest that there is repulsion present between the micelles and the origin of this repulsion is an electrostatic interaction, although the ionic strength is relatively large. When we plotted  $d_m^2$  against  $C_D$ , it seemed that the most linear relationship was obtained compared with other plots; this is consistent with  $d_m$  being related to the inter-wormlike cylinder distance. We observe exactly the same behaviour as reported for polymer–electrolyte and salt free (or low-ionic strength) wormlike micelle solutions (Sommer *et al.*, 2002).

Cannavacciuolo *et al.* (2002) carried out a Monte Carlo simulation on systems consisting of many charged wormlike micelles with excluded volume and electrostatic interactions and concluded that the scattering function becomes almost identical with that of uncharged system when the ionic strength is more than  $0.1 \text{ mol l}^{-1}$ . This is because the electrostatic screening due to added salt is large enough to reduce repulsion between charged micelles. Their model was able to accurately reproduce the structural peak of the scattering function for charged micelles (Sommer *et al.*, 2002). The  $C_D$  dependence of  $d_m$  in Fig. 7 coincides with their calculation.

According to the rheological measurements, slow and distributed relaxations were observed at  $C_D > 0.6 \text{ mol l}^{-1}$  at  $[\text{Na}^+]^* = 0.75$  and  $1.00 \text{ mol l}^{-1}$ . In this region, the  $d_m$  value becomes approximately twice that of  $R_s$ . This feature means that the micelles push each other and thus direct contact between them becomes possible. At  $C_D > 0.7$ , we can expect that  $d_m$  decreases further, which is consistent with the fact that liquid–liquid phase separation takes place at  $C_D > 0.7$ .

## 5. Conclusions

SAXS data on LES/AMPB/water systems were systematically obtained as a function of  $[\text{Na}^+]^*$  and  $C_D$ . The form factor was

experimentally obtained by extrapolating  $I(q)/C_D$  to  $C_D = 0$  and the resultant profiles were well fitted with a core–shell cylinder model for all  $[\text{Na}^+]^*$ . The parameters of  $R_c$ ,  $R_s$  and  $V_c$  were  $1.2 \pm 0.05 \text{ nm}$ ,  $3.1 \pm 0.05 \text{ nm}$  and  $-10$  for all  $[\text{Na}^+]^*$ , indicating that the cross-sectional micelle structure does not depend on the salt concentration.  $S(q)$  was obtained by use of equation (2) and thus  $d_m$  was obtained at the first maximum peak of  $S(q)$ . The  $d_m$  value decreased with increasing  $C_D$  and  $[\text{Na}^+]^*$ . These features indicate that repulsion (presumably due to electrostatic interactions) between the micelles is still present at such high salt concentrations. The rheological measurements had shown presence of slow relaxations in the range of  $C_D > 0.60 \text{ mol l}^{-1}$  for  $[\text{Na}^+]^* = 1.0$  and  $0.75 \text{ mol l}^{-1}$ . In these ranges,  $d_m$  became  $2.5R_s$ .

The present work was supported by Grant-in-Aid for Scientific Research (16350068 & 16655048) and the SAXS was carried out SPring-8 BL40B2 (2005B0150, 2005B0405, 2006A1510, 2006A1534).

## References

- Acharya, D. P., Sato, T., Kaneko, M., Singh, Y. & Kunieda, H. (2006). *J. Phys. Chem. B*, **110**, 754–760.
- Cannavacciuolo, L., Pedersen, J. S. & Schurtenberger, P. (2002). *Langmuir*, **18**, 2922–2932.
- Eguchi, E. & Sakurai, K. (2007). In preparation.
- Ferry, J. D. (1980). *Viscoelastic Properties of Polymers*, 3rd edition. New York: John Wiley & Sons.
- Hiwatari, Y., Yoshida, K., Akutsu, T., Yabu, M. & Iwai, S. (2004). *Int. J. Cosmet. Sci.* **26**, 315–316.
- Jerke, G., Pedersen, J. S., Egelhaaf, S. U. & Schurtenberger, P. (1998). *Langmuir*, **14**, 6013–6024.
- Mu, J. H., Li, G. Z., Jia, X. L., Wang, H. X. & Zhang, G. Y. (2002). *J. Phys. Chem. B*, **106**, 11685–11693.
- Pedersen, J. S. (1997). *Adv. Colloid Interf. Sci.* **70**, 171–210.
- Schurtenberger, P., Magid, L. J., King, S. M. & Lindner, P. (1991). *J. Phys. Chem.* **11**, 4173–4176.
- Shikata, T., Hirata, H. & Kotaka, T. (1987). *Langmuir*, **3**, 1081–1086.
- Shikata, T., Hirata, H. & Kotaka, T. (1988). *Langmuir*, **4**, 354–359.
- Sommer, C., Pedersen, J. S., Egelhaaf, S. U., Cannavacciuolo, L., Kohlbrecher, J. & Schurtenberger, P. (2002). *Langmuir*, **18**, 2495–2505.